USGS AND DLR TOPOGRAPHIC MAPPING OF COMET BORRELLY

E. Howington-Kraus[1], R. Kirk[1], L. Soderblom[1], B. Giese[2], J. Oberst[2]

[1]United States Geological Survey, Astrogeology Team, Flagstaff AZ 86001, US (ahowington,rkirk)@usgs.gov
[2]DLR Institute of Space Sensor Technology and Planetary Exploration, D-12489, Berlin, Germany

Commission IV, WG IV/9

KEY WORDS: Borrelly, comet topographic mapping, photogrammetry, softcopy, extraterrestrial mapping

ABSTRACT:

In the fall of 2001, NASA's Deep Space 1 (DS1) probe imaged Comet Borrelly during a flyby encounter. Three of the Borrelly images have geometry suitable to photogrammetrically map the nucleus, which form two stereopairs with an expected precision (EP) of ~410 m and ~670 m each. DS1 team members at the USGS and DLR have independently produced digital elevation models (DEMs) of Borrelly. Automatic stereo-matching algorithms were used by both USGS and DLR, but the USGS DEM was additionally manually edited in stereo. We accomplished a quantitative statistical comparison of the DEMs and found they have a standard deviation of 120 m, which is small compared to the EP above. There are systematic differences in the DEMs attributable to manual versus automatic matching, but neglecting the systematic differences, we estimate the stereomatching error to only 0.20 pixel RMS, which is similar to the level of subpixel matching accuracy obtained in a wide variety of other mapping situations. The resulting DEMs enable a variety of applications such as perspective views, photometric modeling and studies of the energy balance of the nucleus. We hope to use the USGS DEM as a starting point to extrapolate the shape of the hidden side of the nucleus. This would not only let us determine the volume and moments of inertia of the nucleus, but would lead to a calculation of the insolation onto the nucleus averaged over an entire orbit, and thence to a model of the evolution of nuclear shape.

1. INTRODUCTION

On September 22, 2001, NASA's Deep Space 1 (DS1) probe successfully collected data and imaged Comet Borrelly during a flyby encounter (Figure 1). From a distance of ~90,000 to 3556 kilometers from Borrelly's nucleus, DS1's onboard MICAS (Miniature Integrated Camera and Spectrometer) CCD Sensor captured 20 black-and-white images of Borrelly in a span of 90 minutes (Soderblom et al., 2002). A variety of terrains and surface textures, mountains and fault structures, and darkened material are visible over the nucleus's surface (Britt et al., 2002).

Of the Borrelly images, "near_1" paired with "mid_5_4" and "mid_5_3" make up the optimal stereopairs, having the best compromise between increasing resolution and decreasing convergence angle to photogrammetrically map the nucleus at the highest resolution possible. These images were acquired at a range from the camera of 3556, 3962, and 4387 kilometers, respectively (Figure 1), yielding a ground sample distance of ~46.6 m/pixel for near_1, ~52.0 m/pixel for mid_5_4, and ~57.8 m/pixel for mid_5_3. The expected precision (EP) for stereomodel near_1/mid_5_3 (Figure 2) is ~410 m and that for near_1/mid_5_4 is ~670 m. These precisions are for a stereomatching error of 1 pixel, and smaller errors should be obtainable by automatic matching methods, except in very bland areas. This precision is a small fraction of the dimensions (~8x2 km) of the nucleus, indicating that it should be possible to gen-

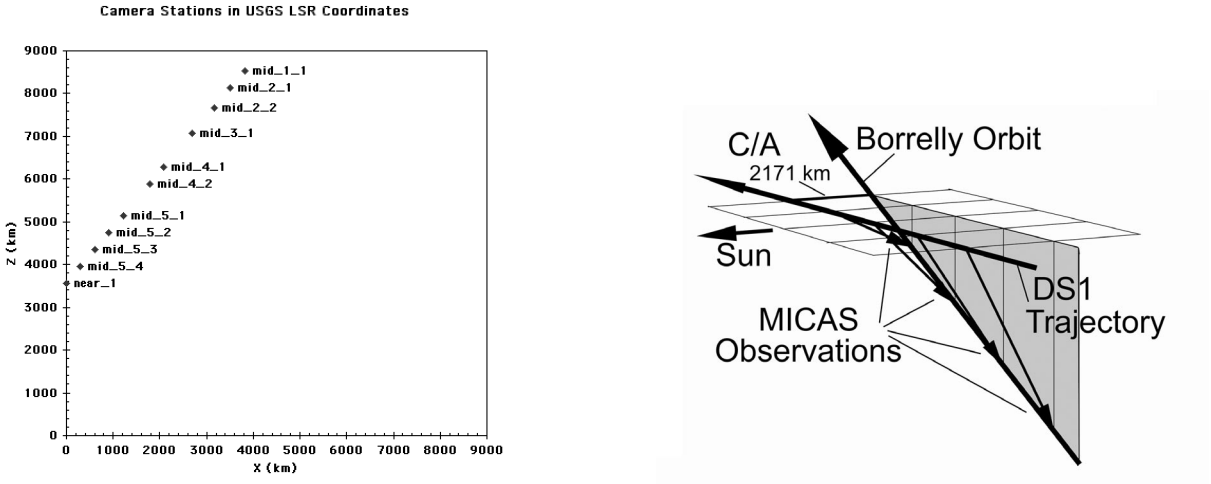

Figure 1. Geometry of DS1 encounter with comet Borrelly. Left, perspective view: spacecraft was looking down on comet nucleus in ecliptic coordinates. Images in this paper are oriented with direction to Sun (shown here by arrow) toward the left. Right, encounter geometry in X-Z plane of Borrelly-fixed LSR coordinates defined for USGS DEM (nucleus is at origin). The Sun is 51° left of the Z axis and ~6° out of the plane of the figure.

erate a relatively detailed stereo digital elevation model (DEM) of Borrelly. DS1 team members at the USGS and DLR have each produced such a model. It is important to note that, though we refer to "elevations" these are not measured in the direction of local gravitational acceleration as commonly understood, or even radially with respect to the center of the Borrelly nucleus. Instead, a Cartesian coordinate system is used, with "elevation" referring to displacement toward the spacecraft, relative to an arbitrary plane. We outline the methodologies used to produce each DEM and present a quantitative statistical comparison and examples of applications.

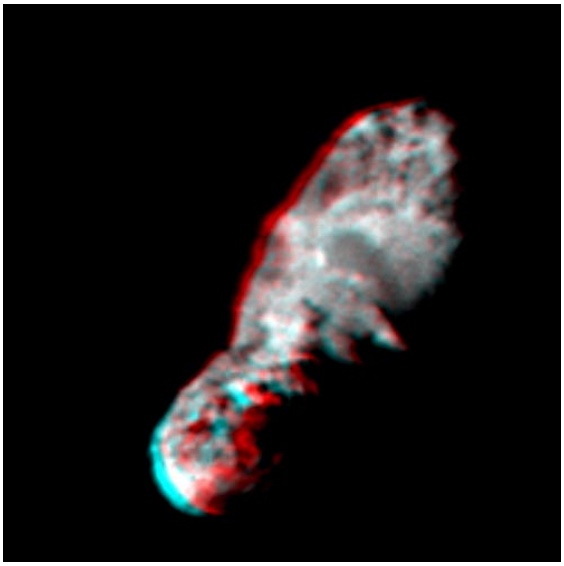

Figure 2. Stereoanaglyph of Borrelly nucleus based on deblurred versions of images near_1 and mid_5_3, which were used for DEM extraction by USGS and DLR. View with red filter on left eye.

2.1 USGS Stereo Analysis

The mapping phase of our work was accomplished on an LH Systems DPW-790 digital photogrammetric workstation running SOCET Set software (© BAE Systems; Miller and Walker, 1993, 1995). Prior to actual mapping, the following preparation steps were accomplished.

• IMAGE PROCESSING: Because the Borrelly images were acquired in a flyby, some are noticeably blurred. Memong Lee of Jet Propulsion Laboratory deblurred the images utilizing an iterative scheme to estimate the combined point spread function from the camera optics and spacecraft motion. Once deblurred, the images were imported into ISIS (Eliason, 1997; Gaddis et al., 1997; Torson and Becker, 1997) where divide and high-pass filters were applied in order to sharpen and even the tone of the images.

• COORDINATE SYSTEM DEFINITION: To topographically map Borrelly in a system related to the comet's surface, we defined an LSR coordinate system having X=Y=0 at a point above the approximate center of mass of the comet, and Z=0 at the image limb. This system uses coordinates with the Z-axis toward the near_1 position, agreeing closely with the system used by DLR.

• IMAGE GEOMETRY: The known camera range and phase angle values were converted to the conventions expected by SOCET Set. Specifically, camera position in the LSR coordinate system and camera orientation angles omega, phi, kappa (rotations around X, Y, Z axes consecutively, going from world to camera) were computed.

With the images enhanced, the LSR coordinate system defined, and image geometry converted to photogrammetric terms, we imported the images into SOCET Set where bundle-adjustment and DEM extraction was performed.

The initial image geometry values calculated aimed the camera centers at the approximate LSR origin, therefore an adjustment of the orientation angles was required to aim the camera center at the defined LSR origin and to maximize superimposition of the images. Using SOCET Set's interactive point measurement tool, we measured 16 conjugate image points; of these, 14 were tie points. The remaining two points were a Z-only control point and horizontal-XY control point that established the origin of the LSR coordinates on Borrelly. Bundle-block adjustment was then performed by holding the camera positions and kappa for all images and only allowing angles omega and phi to adjust.

In order to optimize our chances of success in using SOCET Set's automatic matcher when extracting the DEM, it was necessary to adjust the matching strategy parameters to handle the small (155 x 115 pixel) imaged area of the Borrelly nucleus, and to supply an initial DEM "close" to the surface as a starting point for matching. We then collected a DEM over Borrelly at 150 meters/post (Figure 3) which is an elevation measurement at approximately every 3 image pixels of the highest resolution image, near_1. We manually edited the DEM for blunders and then generated an orthoimage of near_1. The image pair near_1/mid_5_4, which has about half the convergence angle of near_1/mid_5_3, was used to check details of the DEM, especially toward the "bottom" of the frame where the parallax is greatest and details are least clear in mid_5_3.

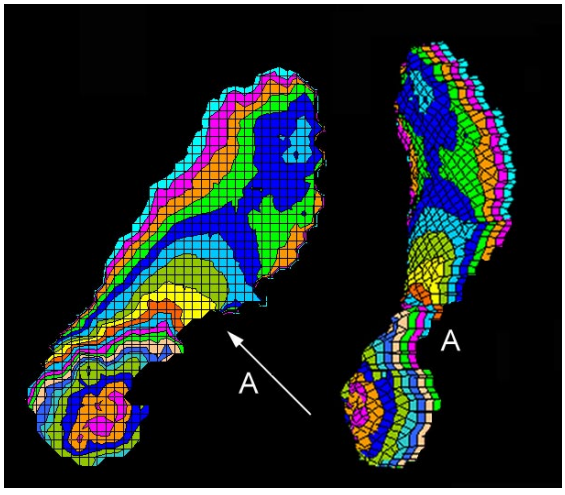

Figure 3. Two views of USGS DEM. Left, view down the Z axis of LSR coordinate system, essentially the same geometry as near_1. Right, view from the direction "A" at 45° from Z axis, no exaggeration. Grid crossings correspond to individual DEM posts with 150 m spacing. Contour interval is 200 m.

2.2 DLR Stereo Analysis

For the purpose of measuring stereo disparities, the deblurred stereo images were radiometrically calibrated and adjusted to have similar sizes, brightness and contrast. Stereo disparities were then measured for a set of 21 individual seed points, using a Zeiss/Phocus stereo system, equipped with a stereo mouse and featuring a 3-D cursor.

In the next step, a computer-based Digital Image Matcher was used to gather disparity points from stereo images near_1 and mid_5_3 (in their original unstretched and not-rotated format) where near_1 was the reference image. The manually collected seed points were used to define the gross perspective distortion of the images and help the matcher start the automatic sampling. Patch sizes of 10–12 pixels were used for the matching, and initial matching runs produced ~8500 disparity points, of which some were off target. After blunder removal, 6990 data points remained.

Owing to the small stereo angle, errors in the estimates for absolute elevations (which are typically made by computing intersection points of the viewing rays) were very large. Instead, the image disparities were converted to relative elevations using a constant conversion factor c, with c = spacecraft range * ifov / stereo angle. Thus, a typical measurement error of 1 pixel in disparity corresponded to an error of 410 m in height (ifov of the MICAS CCD sensor: 13 µrad). However, in some areas, the disparities can be determined to better than 1 pixel, and this error may be smaller. The elevation data were finally interpolated to fill small gaps yielding an estimated accuracy of 500 m horizontally and 150 m vertically.

3. DEM COMPARISON

The DLR and USGS DEMs were collected in different coordinate systems. DLR's DEM is relative to the near_1 image, with an elevation measurement at each near_1 pixel over Borrelly.

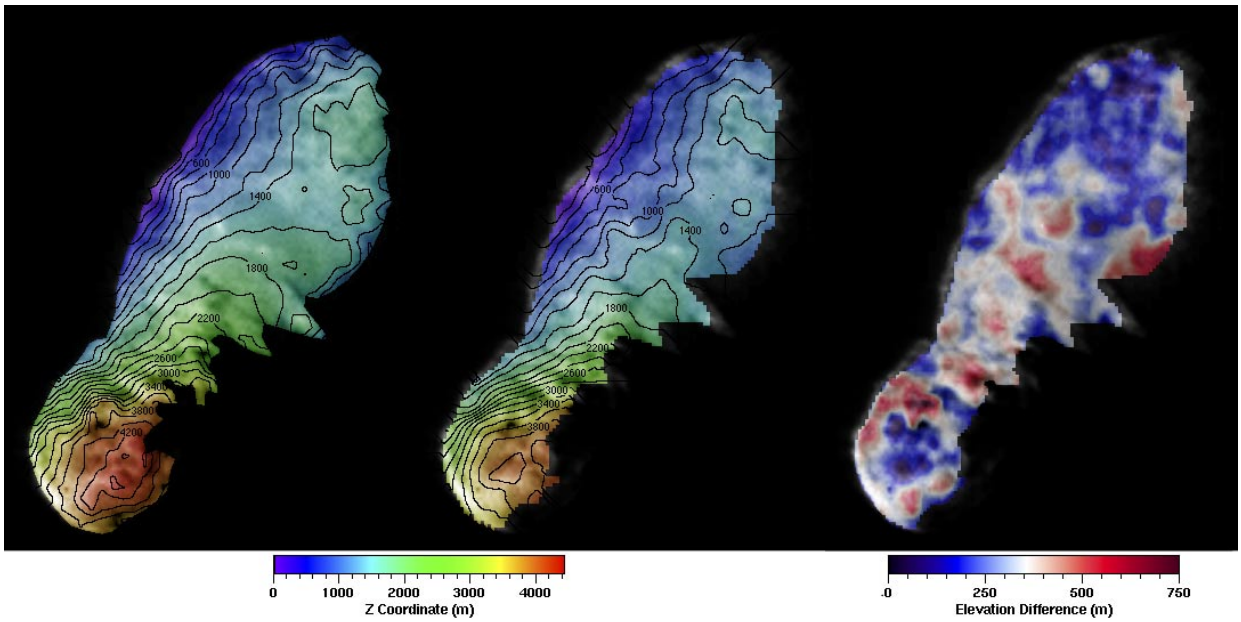

Figure 4. Comparison of USGS (left) and DLR (center) DEMs after alignment in USGS coordinates. Total relief is ~4500 m, contour interval 200 m. Difference (USGS - DLR) is shown at right; average value is arbitrary. USGS model is somewhat less concave than DLR (i.e., higher in the center of the nucleus). This and minor differences in detail and smoothness probably result from the USGS DEM being manually edited after automatic matching.

The USGS DEM is in the above defined LSR coordinates. Therefore, our first step toward comparison was to place the DEMs in the same coordinate system. SOCET Set provides a DEM Registration Tool that scales, translates and rotates the coordinates of one DEM to fit another via an affine transformation, but the DEM coordinates are required to be "close" for successful registration. Unfortunately, our DEMs were not
close enough, so we "manually" scaled the DLR DEM to 48 m/post (the approximate resolution of near_1) and rotated it by 90 degrees around the Z axis. The resulting DEM was "close" to the USGS LSR coordinates so that the fine-tuned registration could be accomplished in SOCET Set.

Figure 4 shows both DEMs overlaid on a rectified version of image near_1 in the USGS coordinate system. The two models are very similar, but the USGS model appears slightly smoother (despite its being based on the deblurred images and the DLR model having been resampled from its original format). Elevations relative to an arbitrary zero (approximately the lowest point on the limb) range to approximately 4600 m, with only a small area above 4000 m. There is a trend from low areas at the "top" to high areas > 3 km at the "bottom". Hence, with its size of 8 km along the longest axis, the "bottom" of the nucleus appears to be tilted toward the camera.

The difference between the two DEMs is also shown in Figure 4. Difference values (USGS - DLR) range from -73 to 825 m with a mean of 300 m and standard deviation 120 m. Because the zero of elevation was set arbitrarily, the mean difference is not of great interest, but the standard deviation is surprisingly small compared to our estimates of precision above. There is a systematic pattern to the difference: the two models agree at the ends of the nucleus but the USGS DEM is higher in the center. This region of the surface is relatively smooth, so the difference may reflect the results of manual versus automatic matching on images that do not have adequate texture. Other differences between the DEMs can probably be related to manual vs. automated collection techniques also. The DLR DEM is smoother at the ends of the nucleus, where the USGS model has been edited to capture troughs in the surface (which are visible in the images as topographic shading); in the blander, center portion, the DLR model is rougher (i.e., noiser) whereas the USGS model has been edited to be relatively smooth.

Neglecting the above complexities, we can obtain an estimate of stereo matching error by attributing the 120 m standard deviation of the difference equally to each DEM. This yields the estimate of 85 m RMS range error. Given the image resolutions and convergence angle, this corresponds to only 0.20 pixel RMS stereomatching error, which is similar to the level of subpixel matching accuracy obtained in a wide variety of other situations. Unfortunately, this achieved precision is marginal to measure the relief of apparent topographic features such as mesas seen in the images (Britt et al., 2002) with any confidence, though these features are reflected in the DEMs to some extent as discussed below. The error in local surface orientation estimates, based on a pair of elevation points 150 m apart, will be ~30°. In order to obtain useful estimates of surface orientation for photometric normalization, thermal balance modeling, etc., it is therefore necessary to average over a relatively large number of DEM points (Oberst et al., 2002).

4. APPLICATIONS

The quantitative models of the Borrelly nucleus enable a variety of interesting investigations; in this paper we show a few examples of work in progress based on the USGS DEM. DLR is using their DEM to study the photometric properties of the nucleus (Oberst et al., 2002).

The DEM can be used to render perspective views of the nucleus as seen from any direction. Simulating images from early in the encounter by reprojecting near_1 data is a convenient way to check for errors in the model. Perspective visualizations are not limited to the geometries of the actual flight track, however. Figure 5 shows three views of the nucleus, two with the geometries of actual images and one looking from the "top" of these frames.

Figure 6 compares the observed image with a Lambert-shaded view of the DEM and a view shaded with a more realistic Minnaert model that was fitted (Kirk et al., 2000) to a Hapke model for C-type asteroid Mathilde (Clark et al., 1999), like Borrelly a very dark objec t. The Lambert model gives a better indication of the details of surface shape (as well as noise in the DEM, which was smoothed with a 5x5 lowpass filter before shading) but the Minnaert model, being slightly limb-brightened, is a better match for the image.

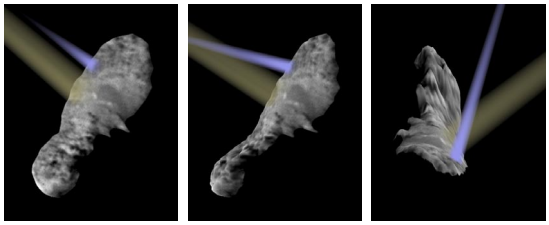

Figure 5. Three perspective views of the nucleus, based on the USGS DEM and near_1 image data. Left, from near_1 camera station; middle, from mid_1_2 station. Right, view from the "top" end of the nucleus (as oriented in the other images). Renderings include schematic representations of the alpha and beta jets (arbitrarily colored yellowish and bluish to distinghish them), based on their inferred 3D geometries (Soderblom et al., 2002). Simulated views like this provide a check on both the DEM and the reconstructed plume geometry.

The correspondence between the models and the image, though imperfect, suggests that some of the image texture is due to relief such as troughs (T) and scarps (S) but some reflects localized albedo variations (A). We are currently pursuing a more quantitative approach to this kind of photometric modeling, including the use of shape-from-shading (photoclinometry) to improve the DEM in bland areas and particularly near the terminator where image radiance is extremely sensitive to surface orientation.

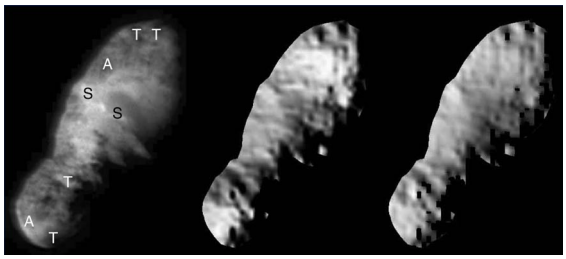

Figure 6. Comparison of radiometrically calibrated image near_1 (left) with images calculated by shading the USGS DEM with a Lambert photometric function (center) and a more realistic, limb-brightened Minnaert function (right). Correspondences (and lack thereof in some areas suggest image shows both topographic features (T=troughs, S=scarps) and local albedo variations (A).

The DEM also has implications for the energy balance of the nucleus. Figure 7 shows the instantaneous insolation and the diurnally averaged insolation, the latter based on the assumption that the alpha jet, whose direction does not change appreciably over time, is aligned with the spin axis of the nucleus (Soderblom et al., 2002). More speculatively, we hope to use the DEM as a starting point to extrapolate the shape of the hidden side of the nucleus. This would not only let us determine the volume and moments of inertia of the nucleus, but would lead to a calculation of the insolation onto the nucleus averaged over an entire orbit, and thence to a model of the evolution of nuclear shape. Obviously, such a program must include a careful assessment of how the results depend on uncertainties in the estimated hidden portion of the nucleus.

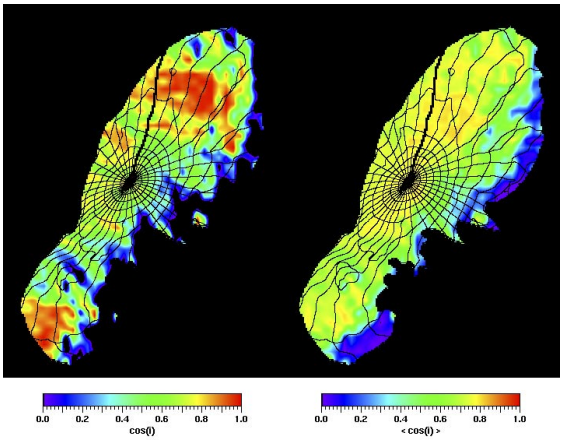

Figure 7. Comparison of instantaneous (left) and diurnally averaged (right) relative insolation onto the nucleus. Cosine of the incidence angle is shown, i.e., model of solar energy input ignores details of photometric function and nonuniform albedo. Overlaid on these models is a 10° (planetocentric) latitude-longitude grid. Coordinate system has polar axis aligned with alpha jet (the assumed axis of rotation (Soderblom et al., 2002)) and prime meridian at the "bottom" end. Location of origin is conjectural, at the approximate center of the nucleus as seen in stereo.

5. REFERENCES

Britt, D. T., et al., 2002. The geology of Comet 19/P Borrelly. *Lunar Planet. Sci*. XXXIII, Abstract #1686, Lunar and Planetary Institute, Houston (CD-ROM).

Clark, B. et al., 1999. NEAR photometry of Asteroid 253 Mathilde. *Icarus*, 140(1), pp. 53-65.

Eliason, E., 1997. Production of digital image models using the ISIS system. *Lunar Planetary Sci*., XXVIII, pp. 331-332, Lunar and Planetary Institute, Houston.

Gaddis, L. et al., 1997. An overview of the Integrated Software for Imaging Spectrometers (ISIS). *Lunar Planetary Sci*., XXVIII, pp. 387-388, Lunar and Planetary Institute, Houston.

Kirk, R. L., Thompson K. T., Becker T. L., and Lee E. M., 2000. Photometric modeling for planetary cartography. *Lunar Planet. Sci*. XXXI, Abstract #2025, Lunar and Planetary Institute, Houston (CD-ROM).

Miller, S. B. and Walker, A. S., 1993. Further developments of Leica digital photogrammetric systems by Helava. *ACSM/ASPRS Annual Convention and Exposition Technical Papers*, 3, pp. 256-263.

Miller, S. B. and Walker, A. S., 1995. Die Entwicklung der digitalen photogrammetrischen Systeme von Leica und Helava. *Z. Photogramm. Fernerkundung*, 1/95, pp. 4-16.

Oberst, J., Giese B., Soderblom L., and the DS1 Science Team, 2002. The nucleus of Comet Borrelly: A study of morphology and surface brightness. *Lunar Planet. Sci*. XXXIII, Abstract #1716, Lunar and Planetary Institute, Houston (CD-ROM).

Soderblom, L. A., et al., 2002. Encounter with Comet 19P/Borrelly: Results from the Deep Space 1 Miniature Integrated Camera and Spectrometer. *Lunar Planet. Sci*. XXXIII, Abstract #1256, Lunar and Planetary Institute, Houston (CD-ROM).

Torson, J. and Becker, K., 1997. ISIS: A software architecture for processing planetay images. *Lunar Planetary Sci*., XXVIII, pp. 1443-1444, Lunar and Planetary Institute, Houston.